UK Atomic Energy Authority

H. J. Campbell, F. Schoofs, A. Reilly
UKAEA-STEP-PR(22)04

Characterisation of the effects of proton irradiation on functional properties of REBCO coated conductor tapes using a Physical Properties Measurement System

Characterisation of the effects of proton irradiation on functional properties of REBCO coated conductor tapes using a Physical Properties Measurement System

H. J. Campbell, F. Schoofs, A. Reilly

This is a preprint of a paper submitted for publication in
Journal of Nuclear Materials

'Characterisation of the effects of proton irradiation on functional properties of REBCO coated conductor tapes using a Physical Properties Measurement System'

Holly Jane Campbell, Frank Schoofs and Aidan Reilly

United Kingdom Atomic Energy Authority, Culham Science Centre, Abingdon, OX14 3DB, U.K.

E-mail address: holly.campbell@ukaea.uk

ICFRM-20 Conference Proceedings Manuscript - From Oral Contribution

Abstract

Rare earth barium copper oxides (REBCO) are a particular class of cuprate high temperature superconductor. The favourable properties of REBCO coated conductor tapes (CCTs) and the well-established production methods have brought these tapes to the forefront of tokamak fusion research, showing a lot of promise for the development of powerful, high field magnets. A current area of research is the effect of irradiation on the functional properties of CCTs. At the UKAEA Materials Research Facility (MRF), a Quantum Design Physical Properties Measurement System (PPMS)® Dynacool™ has recently been installed. The PPMS is a versatile piece of equipment capable of various physical property measurements as a function of magnetic field strength or temperature. The MRF is in the unique position of being able to characterise irradiated/radioactive materials in the PPMS. In this work, measurements in the AC Magnetic Susceptibility operational mode pre- and post-proton irradiation experiments were used to investigate how the functional properties of 2 different CCTs were affected by radiation. The CCT samples were very similar in their overall composition but had different flux-pinning landscapes, and it was this variable which led to differences in performance prior to irradiation and in radiation tolerance. A major conclusion was that future CCTs in fusion applications will need to find a balance between low temperature critical current density enhancement and performance under irradiation.

Key words

Fusion magnets, REBCO, CCTs, PPMS, proton irradiation

Introduction

REBCO materials are a particular class of cuprate high temperature superconductor. The most well-known rare-earth barium copper oxide is YBCO with yttrium as the rare earth, but other common examples contain dysprosium (DyBCO), europium (EuBCO), samarium (SmBCO) and gadolinium (GdBCO).[1-3]

Recent improvements in the achievable critical current densities (J_c) of REBCO coated conductor tapes (CCT), together with the high upper critical magnetic fields (B_{c2}) and critical temperatures (T_c) of REBCO make these tapes very attractive for demanding, high applied field or current applications.[4] The favourable properties of REBCO CCTs and the well-established production methods have brought these tapes to the forefront of tokamak fusion research.[5]

Footnote:
SuperPower SF4050-AP-i CCT composition: 2 µm silver overlayer; 1.6 µm YBCO layer containing $BaZrO_3$ nano-column artificial pinning centres deposited by metal-organic chemical vapour deposition; 0.2 µm biaxially-textured MgO buffer stack deposited by ion beam assisted deposition; 50 µm Hastelloy substrate
Theva TPL1120 CCT composition: 1 µm silver overlayer; 3.5 µm pure GdBCO layer deposited by pulsed vapour deposition; 3.5 µm biaxially-textured MgO buffer stack deposited by inclined substrate deposition; 50 µm Hastelloy substrate

In previous work discussed in literature, proton irradiation was found to introduce mainly oxygen and some copper Frenkel pair point defects in REBCO.[6-10] The introduction of high densities of point defects causes a crossover in the overall flux-pinning mechanism, from strong individual pinning by artificial pinning centres, stacking faults, dislocations etc. already present in the pristine REBCO microstructure, to weak collective pinning by point defects.[6] A primary cause of this crossover is the reduction in the *ab*-axis coherence length caused by oxygen displacement within the superconducting CuO_2 planes of REBCO.[11]

The coherence length is spatially dependent, and therefore increasing densities of oxygen vacancies with proton fluence leads to a reduced coherence length over more of the REBCO thin film in CCTs. Overall, this causes a decrease in the pinning capability of the larger nm-scale microstructural defects, resulting in a lower activation energy for de-pinning of flux, which in turn increases the rate of flux flow.[12][13] Point defects then dominate the pinning landscape, and due to the weak pinning force of point defects, consequently proton irradiation degrades J_c in REBCO CCTs.

Current research is trying to establish the potential optimal flux-pinning landscape for REBCO CCTs in fusion applications.[5] The goal would be for operational J_c values to be maintained over long periods of time under fusion conditions due to superior radiation tolerance. Magnetometry measurements before and after irradiation experiments may be used to evaluate changes in critical superconducting parameters. Characterisation of proton-irradiated CCTs with different flux-pinning landscapes was the focus of this work, with the intention of comparing the relationship between the pristine pinning landscape and subsequent radiation tolerance in the different tapes.

Experimental

Proton irradiation experiments were carried out at the Dalton Cumbrian Facility. Samples were irradiated with 2.5 MeV protons using a beam current of 4.5 µA up to a maximum fluence of 6×10^{20} p^+/m^2. During irradiation, the temperature of the samples was maintained below 373 K.

Two coated conductor tape samples were investigated in this study, the **SuperPower SF4050-AP-i** and **Theva TPL1120**. The major difference between the two tapes is the as-received flux-pinning landscape in the REBCO layers. The inclined substrate deposition technique used for deposition of the MgO buffer stack in the TPL1120 tape results in the GdBCO *c*-axis having a 30 ^{o} tilt with respect to the tape surface normal.

Characterisation of the CCT samples pre- and post-irradiation involved magnetometry measurements in the AC magnetic susceptibility operational mode of the Quantum Design PPMS® DynaCool™ Measurement System at the UKAEA Materials Research Facility. The PPMS in the Materials Research Facility is intended for characterisation of functional properties in radioactive/irradiated materials. For all measurements, 3 mm disks were cut from the tapes prior to irradiation using a SPI Supplies #17001-AB precision 3 mm TEM disk punch and magnetic fields were applied perpendicular to the tape surface (parallel to YBCO *c*-axis in the SF4050-AP-i tape and 30 ^{o} tilted from GdBCO *c*-axis in the TPL1120 tape). For AC susceptibility measurements, a 0.001 T AC drive was applied.

Values for magnetisation critical current densities were calculated from magnetic moment versus applied magnetic field hysteresis loops using Bean's critical state model for a thin film.[14]

Footnote:
SuperPower SF4050-AP-i CCT composition: 2 µm silver overlayer; 1.6 µm YBCO layer containing $BaZrO_3$ nano-column artificial pinning centres deposited by metal-organic chemical vapour deposition; 0.2 µm biaxially-textured MgO buffer stack deposited by ion beam assisted deposition; 50 µm Hastelloy substrate
Theva TPL1120 CCT composition: 1 µm silver overlayer; 3.5 µm pure GdBCO layer deposited by pulsed vapour deposition; 3.5 µm biaxially-textured MgO buffer stack deposited by inclined substrate deposition; 50 µm Hastelloy substrate

Results and Discussion

SuperPower SF4050-AP-i

AC Susceptibility

Below in Figure 1 is the AC susceptibility profile for the control SF4050-AP-i sample. The profile is typical of a superconductor, with maximum T_c (~90 K) in the absence of an applied magnetic field and an observed decrease in T_c as applied field increased.

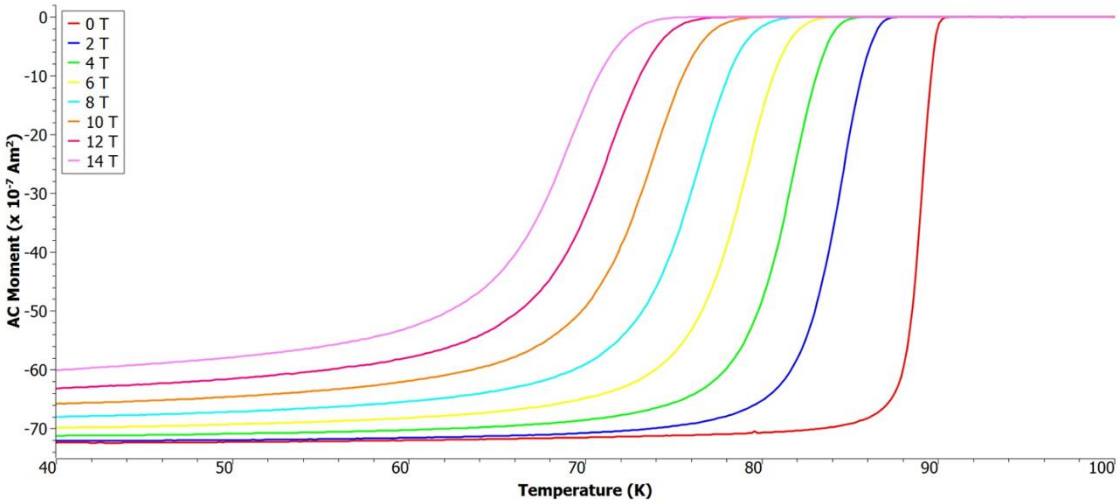

Fig. 1 AC magnetic moment versus temperature profile for the control SF4050-AP-i CCT sample at various applied magnetic field strengths.

The AC susceptibility profile for the SF4050-AP-i sample which had been irradiated to 3 x 10^{20} p^+/m^2 is shown in Figure 2. This profile does not indicate a superconducting transition. The substrate, which makes up the bulk of a CCT, is composed of Hastelloy® C-276™.[15] Hastelloy is a poor conductor, and the weak diamagnetic signal in the presence of a time-varying AC drive field is suggestive of induced eddy currents.

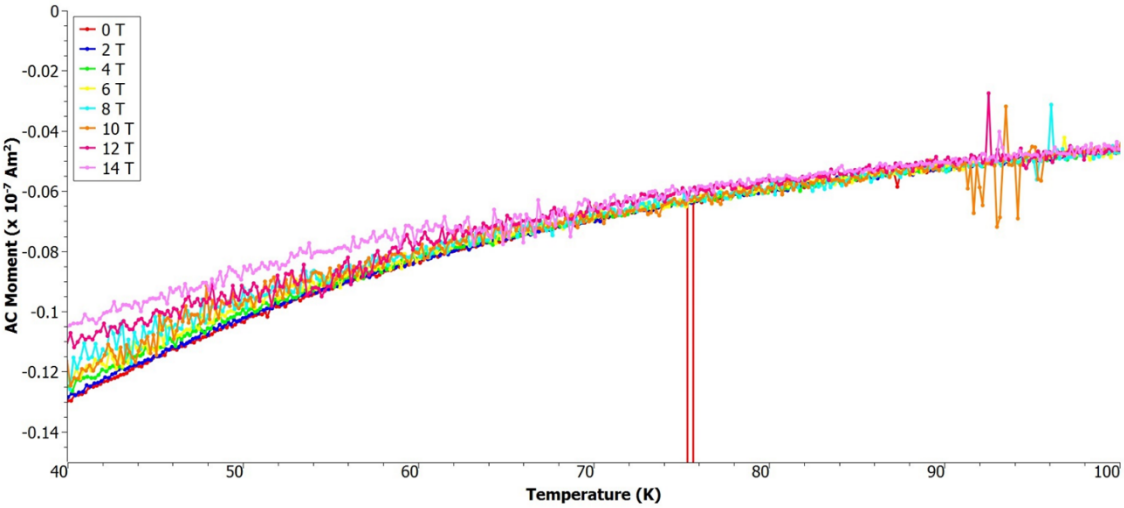

Fig. 2 AC magnetic moment versus temperature profile for the SF4050-AP-i CCT sample that had been irradiated to 3 x 10^{20} p^+/m^2 at various applied magnetic field strengths. The data points around 95 and 75 K within the respective datasets are likely due to noise/an error in picking up the sample signal.

Footnote:
SuperPower SF4050-AP-i CCT composition: 2 µm silver overlayer; 1.6 µm YBCO layer containing $BaZrO_3$ nano-column artificial pinning centres deposited by metal-organic chemical vapour deposition; 0.2 µm biaxially-textured MgO buffer stack deposited by ion beam assisted deposition; 50 µm Hastelloy substrate
Theva TPL1120 CCT composition: 1 µm silver overlayer; 3.5 µm pure GdBCO layer deposited by pulsed vapour deposition; 3.5 µm biaxially-textured MgO buffer stack deposited by inclined substrate deposition; 50 µm Hastelloy substrate

DC-Extraction

Using Bean's critical state model, the magnetic hysteresis data (Figure 3) was used to calculate the magnetisation J_c as a function of applied magnetic field strength (Figure 4).

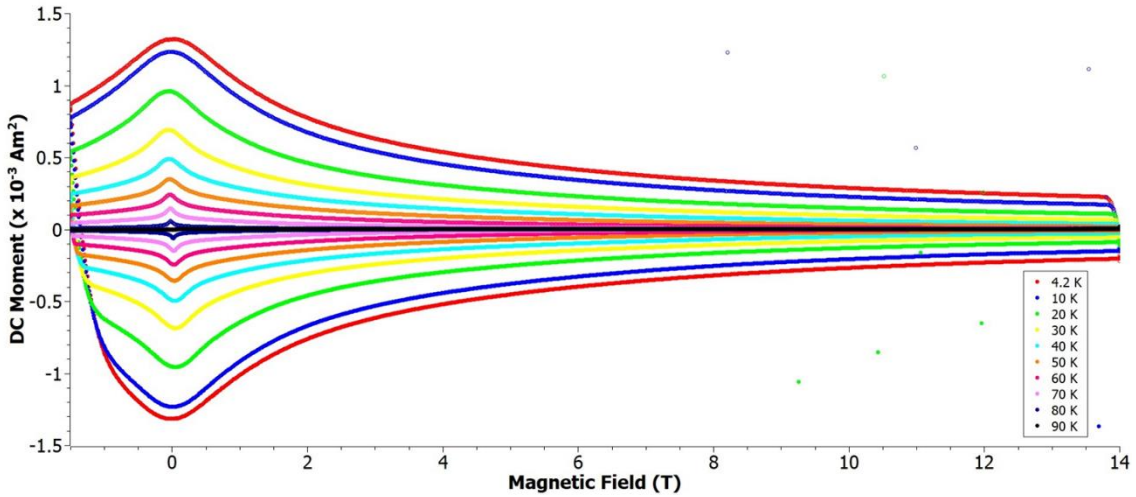

Fig. 3 DC magnetic moment versus applied magnetic field profile for the control SF4050-AP-i CCT sample at various temperatures.

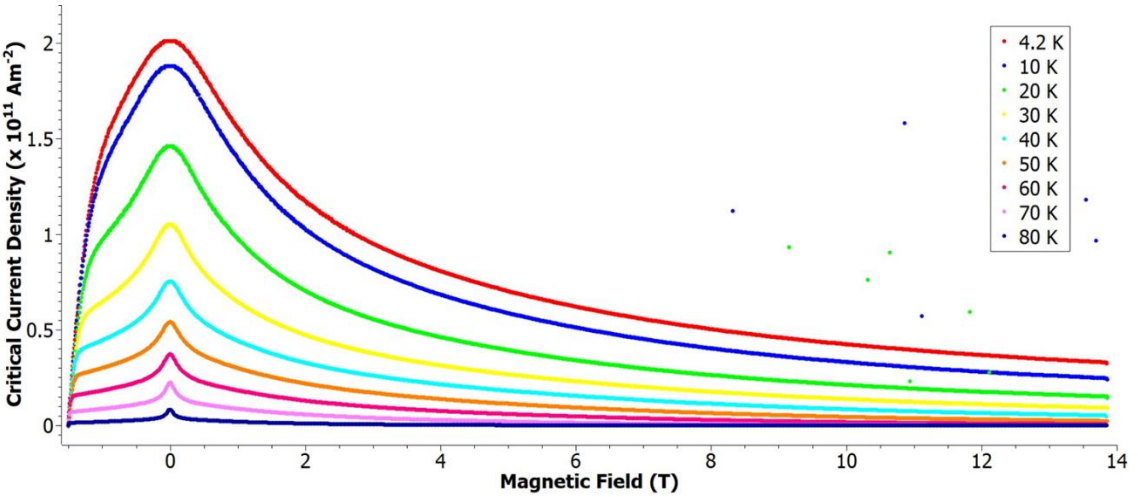

Fig. 4 Magnetisation critical current density versus applied magnetic field profile for the control SF4050-AP-i CCT sample at various temperatures.

The DC-extraction profile for the SF4050-AP-i sample which had been irradiated to 3 x 10^{20} p^+/m^2 (Figure 5), like the AC susceptibility profile, demonstrated the absence of superconductivity. Hastelloy is paramagnetic in static DC fields, which is conducive to the positive susceptibility, lack of hysteresis and the sinusoidal shape of the signal seen in the profile.[15] It was concluded from both the AC and DC measurement data that after irradiation to the fluence 3 x 10^{20} p^+/m^2, superconductivity had been destroyed in the SF4050-AP-i CCT.

Footnote:
SuperPower SF4050-AP-i CCT composition: 2 µm silver overlayer; 1.6 µm YBCO layer containing $BaZrO_3$ nano-column artificial pinning centres deposited by metal-organic chemical vapour deposition; 0.2 µm biaxially-textured MgO buffer stack deposited by ion beam assisted deposition; 50 µm Hastelloy substrate
Theva TPL1120 CCT composition: 1 µm silver overlayer; 3.5 µm pure GdBCO layer deposited by pulsed vapour deposition; 3.5 µm biaxially-textured MgO buffer stack deposited by inclined substrate deposition; 50 µm Hastelloy substrate

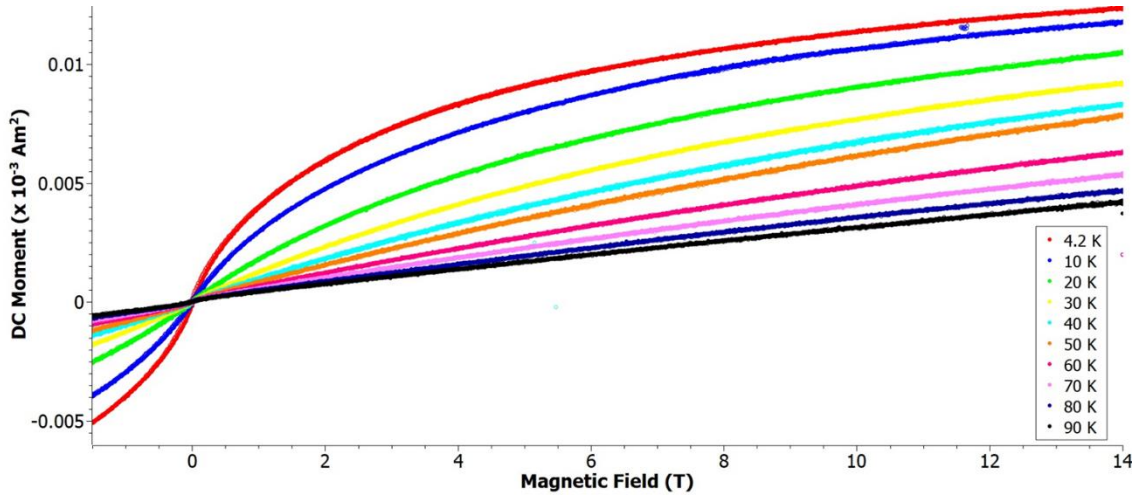

Fig. 5 DC magnetic moment versus applied magnetic field profile for the SF4050-AP-i CCT sample that had been irradiated to 3 x 10^{20} p^+/m^2 at various temperatures.

Theva TPL1120

AC Susceptibility

Unlike the control SF4050-AP-i CCT, the control TPL1120 sample maintained almost full diamagnetic saturation even under 14 Tesla field in its AC susceptibility profile (Figure 6). This is demonstrated by the flattening out of the curves at low temperatures and only minimal differences in minimum moment under applied field. At low fields, the AC profiles for both the control tape samples have almost identical minima points, and similar values for T_c are observed across all the applied fields. Above 6 Tesla, the profile minima diverge, and as applied field increases towards 14 Tesla, the SF4050-AP-i negative signal decreases by about a seventh relative to the TPL1120 negative signal (Figure 7). From these data, it was inferred that the control TPL1120 CCT maintains stronger diamagnetic shielding under applied fields than the control SF4050-AP-i CCT.

In the TPL1120 tape, there is a pure GdBCO layer, whilst the SF4050-AP-i tape contains artificial pinning centres (APCs) within the YBCO layer. Hence it is likely that the SF4050-AP-i tape therefore pins more flux within its YBCO layer compared to the pure GdBCO. The pinning of flux in type II superconductors causes zero-field cooled magnetometry profiles to have a stronger diamagnetic signal compared to field cooled magnetometry profiles, which means that samples frequently have greater superconducting volume fractions under high fields than suggested by data.[16] Stronger flux-pinning in the SF4050-AP-i tape is therefore the most probable cause of the reduced diamagnetic saturation in the control sample under applied fields.

Footnote:
SuperPower SF4050-AP-i CCT composition: 2 µm silver overlayer; 1.6 µm YBCO layer containing $BaZrO_3$ nano-column artificial pinning centres deposited by metal-organic chemical vapour deposition; 0.2 µm biaxially-textured MgO buffer stack deposited by ion beam assisted deposition; 50 µm Hastelloy substrate
Theva TPL1120 CCT composition: 1 µm silver overlayer; 3.5 µm pure GdBCO layer deposited by pulsed vapour deposition; 3.5 µm biaxially-textured MgO buffer stack deposited by inclined substrate deposition; 50 µm Hastelloy substrate

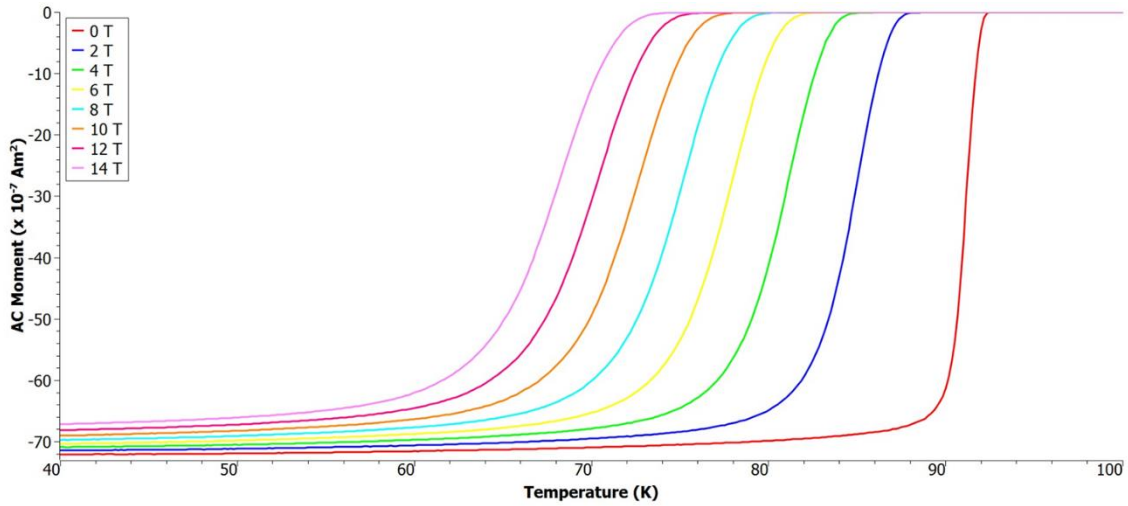

Fig. 6 AC magnetic moment versus temperature profile for the control TPL1120 CCT sample at various applied magnetic field strengths.

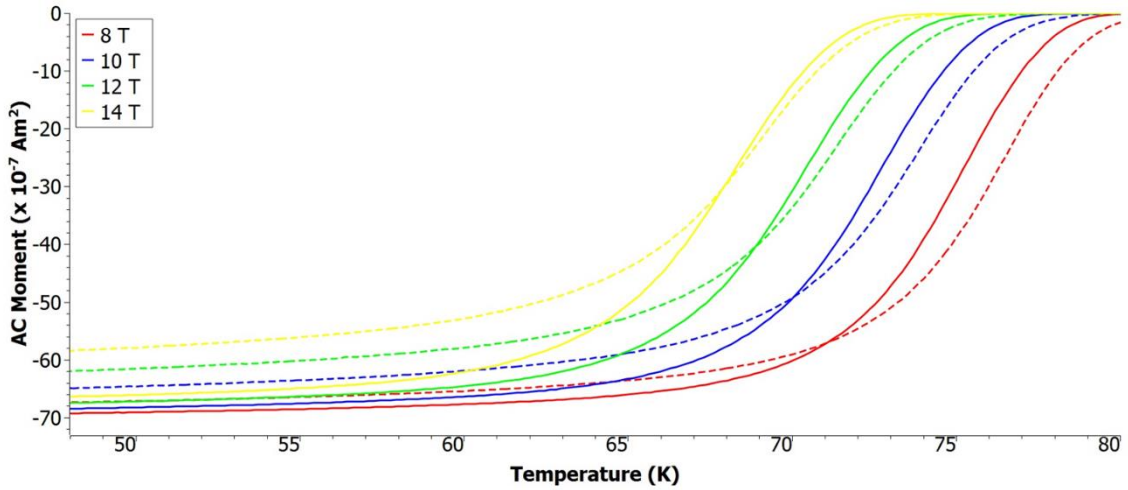

Fig. 7 Comparison of AC magnetic moment versus temperature profiles for the control TPL1120 (solid lines) and control SF4050-AP-i (dashed lines) CCT samples at high applied magnetic field strengths.

For the TPL1120 sample which had been irradiated to 6 x 10^{20} p^+/m^2, full diamagnetic saturation was not seen in the AC susceptibility profile (Figure 8). The minima did not flatten out and the minimum moments were also weaker (Figure 9). However, looking at the shifts in T_c, irradiation did not have a great effect. At 0 field, there was only a few degrees Kelvin decrease, and at 14 Tesla there was about an 8 K reduction.

Footnote:
SuperPower SF4050-AP-i CCT composition: 2 µm silver overlayer; 1.6 µm YBCO layer containing $BaZrO_3$ nano-column artificial pinning centres deposited by metal-organic chemical vapour deposition; 0.2 µm biaxially-textured MgO buffer stack deposited by ion beam assisted deposition; 50 µm Hastelloy substrate
Theva TPL1120 CCT composition: 1 µm silver overlayer; 3.5 µm pure GdBCO layer deposited by pulsed vapour deposition; 3.5 µm biaxially-textured MgO buffer stack deposited by inclined substrate deposition; 50 µm Hastelloy substrate

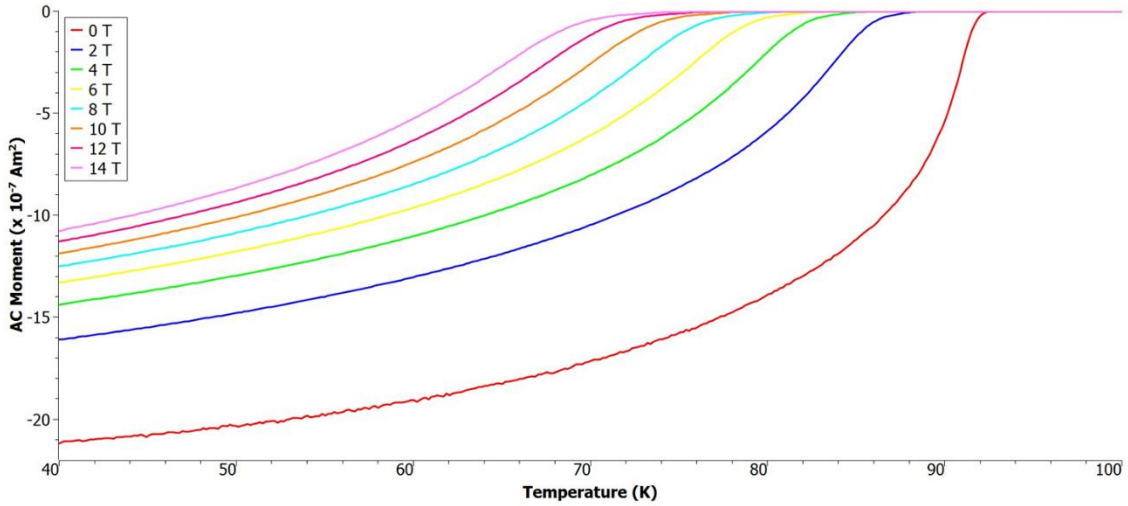

Fig. 8 AC magnetic moment versus temperature profile for the TPL1120 CCT sample that had been irradiated to 6 x 10^{20} p^+/m^2 at various applied magnetic field strengths.

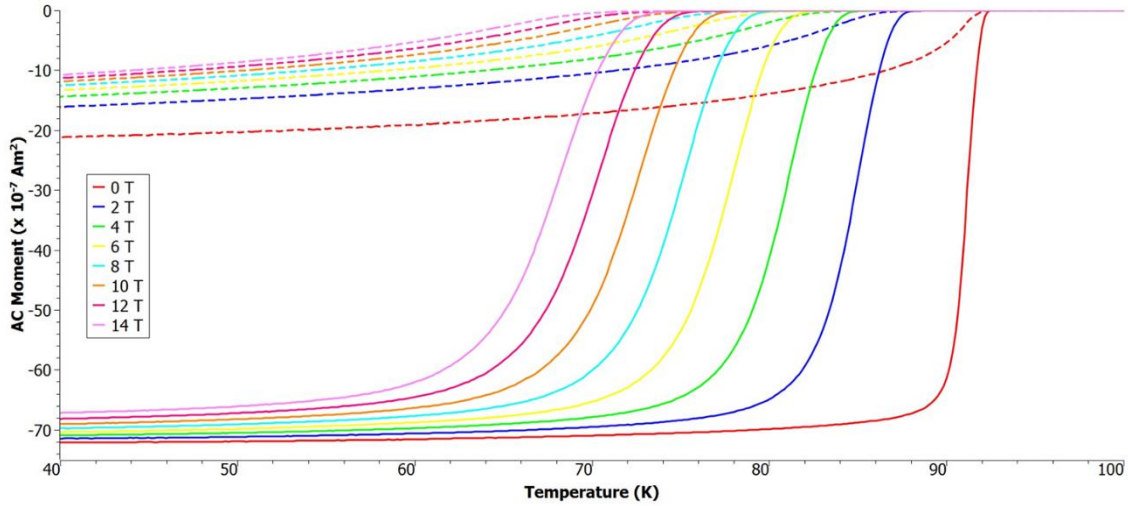

Fig. 9 Comparison of AC magnetic moment versus temperature profiles for the control (solid lines) and irradiated to 6 x 10^{20} p^+/m^2 (dashed lines) TPL1120 CCT samples at various applied magnetic field strengths.

DC-Extraction

The magnetic hysteresis loop for the control TPL1120 sample included 4 'hump' features around 0 field and at low temperatures (asymmetric along the *x*-axis of the plot but mirror images diagonally across the *y*-axis in Figure 10). The GdBCO layer in the TPL1120 tape is deposited such that the *c*-axis is 30 ^{o} off from perpendicular to the tape surface. Changing the direction of the applied field, as is the case during a hysteresis loop measurement, whilst the strong flux-pinning in the *c*-axis is offset from alignment with the field could explain the appearance of these unusual features. The symmetry of the 'humps' observed diagonally across the *y*-axis could then be rationalised by considering the usual symmetry observed in REBCO hysteresis loops along the *y*-axis due to flux-pinning. As temperature increases, the *x*-axis double feature asymmetry is lost, which again could be attributed to changes in pinning force with temperature (there is a reduction in total pinned flux as temperature increases).

Footnote:
SuperPower SF4050-AP-i CCT composition: 2 µm silver overlayer; 1.6 µm YBCO layer containing $BaZrO_3$ nano-column artificial pinning centres deposited by metal-organic chemical vapour deposition; 0.2 µm biaxially-textured MgO buffer stack deposited by ion beam assisted deposition; 50 µm Hastelloy substrate
Theva TPL1120 CCT composition: 1 µm silver overlayer; 3.5 µm pure GdBCO layer deposited by pulsed vapour deposition; 3.5 µm biaxially-textured MgO buffer stack deposited by inclined substrate deposition; 50 µm Hastelloy substrate

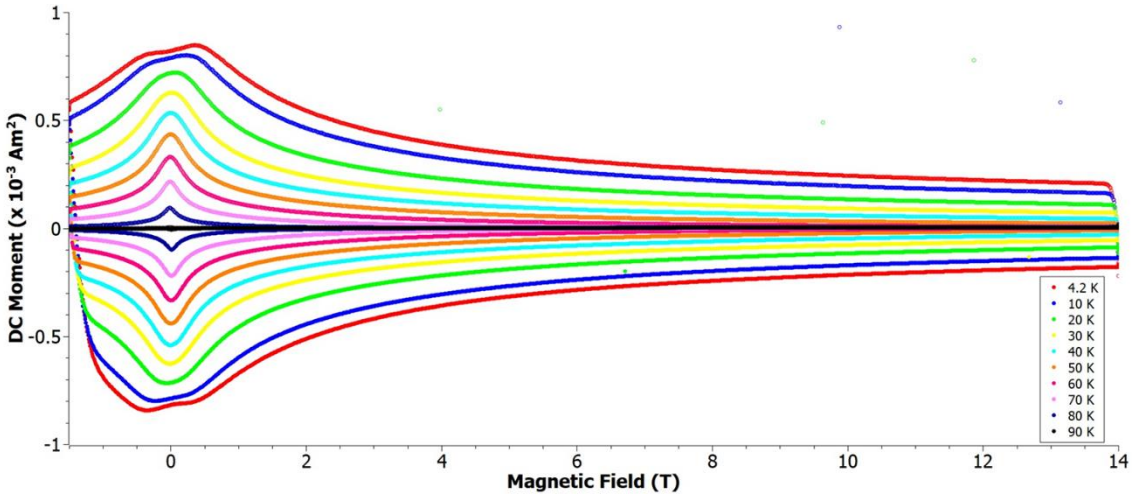

Fig. 10 DC magnetic moment versus applied magnetic field profile for the control TPL1120 CCT sample at various temperatures.

In the TPL1120 tape, there is no artificial enhancement of flux-pinning, therefore J_c is significantly lower than in the SF4050-AP-i tape (Figure 11). At 4.2 Kelvin, the $BaZrO_3$ APCs in the control SF4050-AP-i tape double J_c compared to the control TPL1120 tape (Figure 12). However as temperature increases, the enhancement in J_c decreases, and above 60 Kelvin, both CCTs have similar J_c values at 0 Tesla. That is because as temperature increases, less flux can be pinned within REBCO due to weakened pinning forces, therefore the presence of APCs becomes less important.

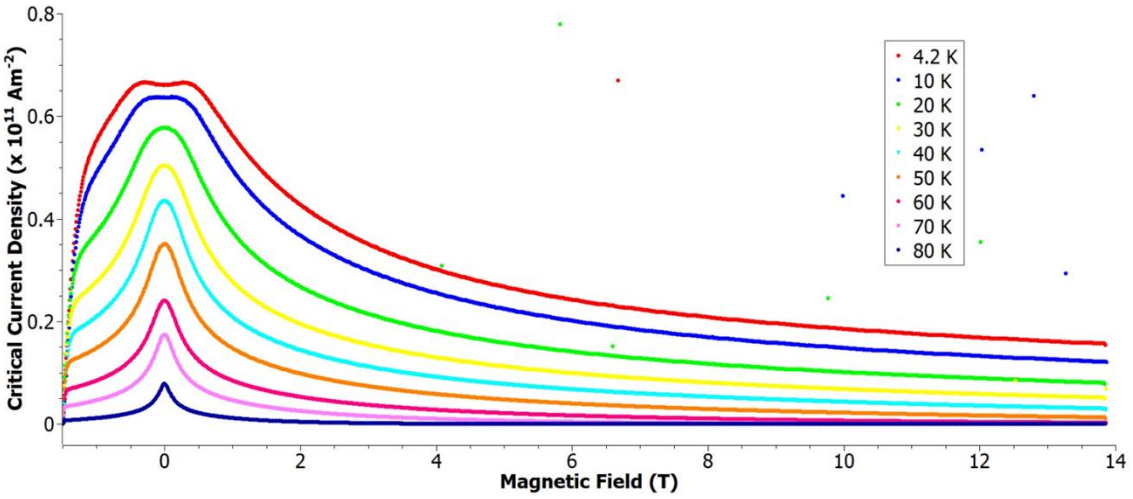

Fig. 11 Magnetisation critical current density versus applied magnetic field profile for the control TPL1120 CCT sample at various temperatures.

Footnote:
SuperPower SF4050-AP-i CCT composition: 2 µm silver overlayer; 1.6 µm YBCO layer containing $BaZrO_3$ nano-column artificial pinning centres deposited by metal-organic chemical vapour deposition; 0.2 µm biaxially-textured MgO buffer stack deposited by ion beam assisted deposition; 50 µm Hastelloy substrate
Theva TPL1120 CCT composition: 1 µm silver overlayer; 3.5 µm pure GdBCO layer deposited by pulsed vapour deposition; 3.5 µm biaxially-textured MgO buffer stack deposited by inclined substrate deposition; 50 µm Hastelloy substrate

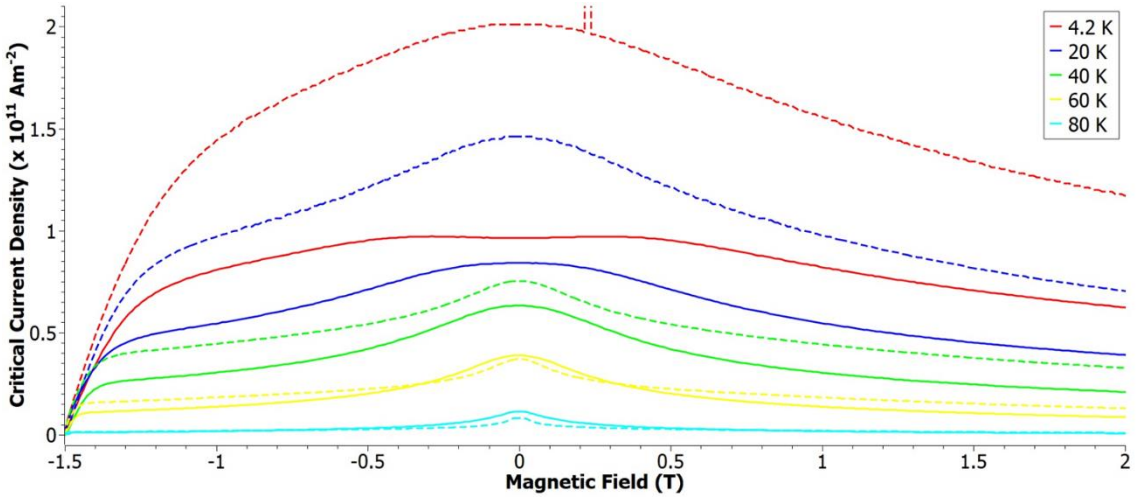

Fig. 12 Comparison of magnetisation critical current density versus applied magnetic field profiles for the control TPL1120 (solid lines) and control SF4050-AP-i (dashed lines) CCT samples at various temperatures.

After irradiation to 6 x 10^{20} p^+/m^2, the upper critical magnetic field appears to have been brought down to about 14 Tesla even at 4.2 Kelvin (Figure 13). Proton irradiation also reduced the moment maxima/minima by an order of magnitude. This decrease was caused by the transition in overall pinning mechanism to weak collective due to the introduction of large numbers of point defects. Only 2 'hump' features (symmetric diagonally across the *y*-axis) are observed in the moment maxima/minima after irradiation. This is likely due to a reduction in anisotropic flux-pinning, previously dominated by e.g. 2D stacking faults, 1D dislocations etc.[17] in the pristine TPL1120 sample, as a consequence of the decrease in pinning force of nm-scale defects. The result is more isotropic pinning associated with 0D point defects.

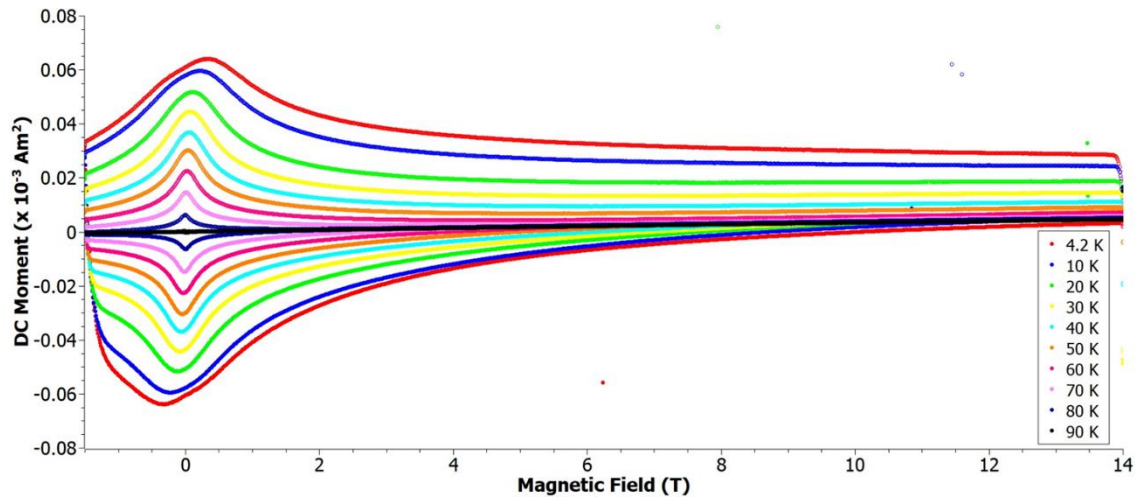

Fig. 13 DC magnetic moment versus applied magnetic field profile for the TPL1120 CCT sample that had been irradiated to 6 x 10^{20} p^+/m^2 at various temperatures.

J_c decreased by an order of magnitude in the TPL1120 tape after irradiation to 6 x 10^{20} p^+/m^2 (Figure 14). However, these results suggested that even after relatively high doses of irradiation, up to double the fluence that that destroyed superconductivity in the SF4050-AP-i tape (3 x 10^{20} p^+/m^2), the TPL1120 CCT can maintain good performance at low temperature.

Footnote:
SuperPower SF4050-AP-i CCT composition: 2 µm silver overlayer; 1.6 µm YBCO layer containing $BaZrO_3$ nano-column artificial pinning centres deposited by metal-organic chemical vapour deposition; 0.2 µm biaxially-textured MgO buffer stack deposited by ion beam assisted deposition; 50 µm Hastelloy substrate
Theva TPL1120 CCT composition: 1 µm silver overlayer; 3.5 µm pure GdBCO layer deposited by pulsed vapour deposition; 3.5 µm biaxially-textured MgO buffer stack deposited by inclined substrate deposition; 50 µm Hastelloy substrate

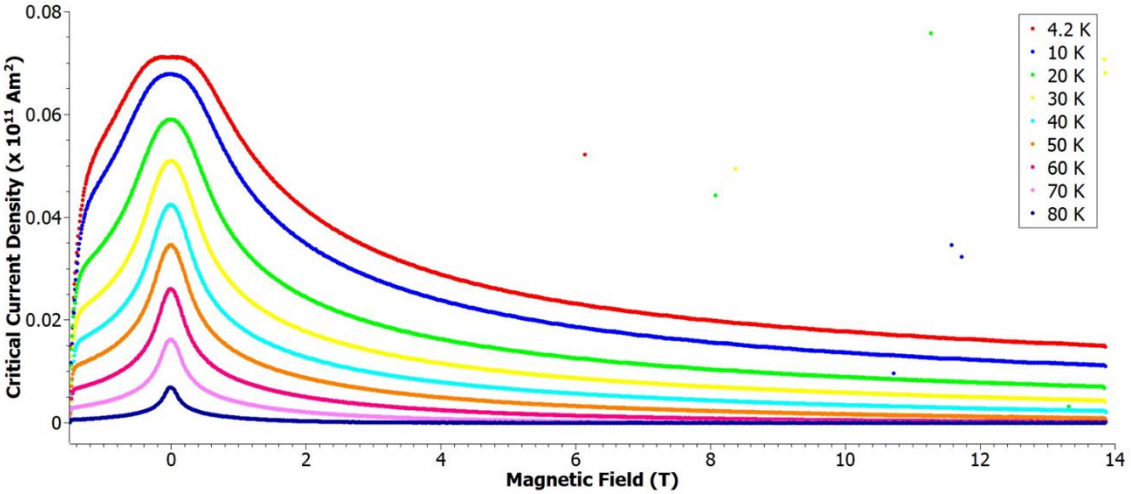

Fig. 14 Magnetisation critical current density versus applied magnetic field profile for the TPL1120 CCT sample that had been irradiated to 6 x 10^{20} p^+/m^2 at various temperatures.

Conclusion

The SuperPower SF4050-AP-i tape had very high J_c at low temperatures because of the $BaZrO_3$ APCs present in the YBCO layer, but this APC enhancement of J_c was only effective at low temperatures. The pure GdBCO in the Theva TPL1120 tape also exhibited better performance under irradiation.

An interesting takeaway is that the $BaZrO_3$ APCs which improve performance in pristine tapes hinder the CCT under irradiation, causing the CCT to become more susceptible to radiation damage. This corroborates observations in literature that when nanoparticle APCs are surrounded by high densities of irradiation-induced defects, the activation barrier for Abrikosov vortex depinning from the nanoparticles decreases significantly.[11] Nanoparticle APCs have very high pinning energies, whilst defect clusters or collision cascades have high pinning energies likely on the order of dislocations, stacking faults etc., and Frenkel pair point defects have very low pinning energies.[11-13][17] Proton irradiation introduces large quantities of point defects, and the dramatic shift in overall pinning mechanism in combination with the drop in individual pinning forces could explain the rapid onset of superconductivity loss in the SF4050-AP-i CCT.[6-10]

CCTs in fusion applications will therefore need to find a balance between low temperature J_c enhancement by APCs and performance under irradiation.

Acknowledgements

The authors thank the Dalton Cumbrian Facility (DCF) for allocating beamline time for the proton irradiation experiments, as well as SuperPower and Theva for providing the CCT samples. The authors would also like to thank the European Physical Sciences Research Council (EPSRC) (grant reference: EP/T012250/1) for providing funding for the work at DCF. This work has been part-funded by STEP, a UKAEA programme to design and build a prototype fusion energy plant and a path to commercial fusion. The research used UKAEA's Materials Research Facility, which has been funded by and is part of the UK's National Nuclear User Facility and Henry Royce Institute for Advanced Materials.

Footnote:
SuperPower SF4050-AP-i CCT composition: 2 µm silver overlayer; 1.6 µm YBCO layer containing $BaZrO_3$ nano-column artificial pinning centres deposited by metal-organic chemical vapour deposition; 0.2 µm biaxially-textured MgO buffer stack deposited by ion beam assisted deposition; 50 µm Hastelloy substrate
Theva TPL1120 CCT composition: 1 µm silver overlayer; 3.5 µm pure GdBCO layer deposited by pulsed vapour deposition; 3.5 µm biaxially-textured MgO buffer stack deposited by inclined substrate deposition; 50 µm Hastelloy substrate

References

[1] J. P. Attfield, J. Mater. Chem. (2011), 21, 4756

[2] Bianconi, D. Di Castro, N. Saini, G. Bianconi (2002), 'Superstripes' In: M. F. Thorpe and J. C. Philips (eds) 'Phase Transitions in and Self-Organisation in Electronic and Molecular Networks', Fundamental Materials Research Book Series, Springer Boston MA

[3] W. K. Kwok, U. Welp, A. Glatz, A. E. Koshelev, K. J. Kihlstrom and G. W. Crabtree, Rep. Prog. Phys. (2016), 79, 116501

[4] P. Bruzzone, W. H. Fietz, J. V. Minervini, M. Novikov, N. Yanagi, Y. Zhai and J. Zheng, Nucl. Fusion (2018), 58, 103001

[5] T. S. Lee, I. Jenkins, E. Surrey and D. P. Hampshire, Fusion Eng. Des. (2015), 98-99, 1072

[6] W. J. Choi, D. Ahmad, Y. I. Seo, R. K. Ko and Y. S. Kwon, Scientific Reports (2020), 10, 2017

[7] B. Egner, J. Geerk, H. C. Li, G. Linker, O. Meyer and B. Strehlau, Jpn. J. Appl. Phys. (1987), 26, 2141

[8] L. Antonova, T. Demikhov, A. Troitskii, A. Didyk, A. Kobzev, A. Yurasov, S. Samoilenkov and G. Mikhailova, Phys. Status Solidi (2015), 12, 94

[9] Y. Jia, M. LeRoux, D. J. Miller, J. G. Wen, W. K. Kwok, U. Welp, M. W. Rupich, X. Li, S. Sathyamurthy, S. Fleshler, A. P. Malozemoff, A. Kayani and O. Alaya-Valenzuela, Appl. Phys. Lett. (2013), 103, 122601

[10] G. C. Xiong, H. C. Li, G. Linker and O. Meyer, Phys. Rev. B (1988), 38, 240

[11] S. Eley, M. LeRoux, M. W. Rupich, D. J. Miller, H. Sheng, P. M. Niraula, A. Kayani, U. Welp, W. K. Kwok and L. Civale, Supercond. Sci. Technol. (2017), 30, 015010

[12] J. Hua, U. Welp, J. Schlueter, A. Kayani, Z. L. Xiao, G. W. Crabtree and W. K. Kwok, Phys. Rev. B (2010), 82, 024505

[13] T. Matsushita, G. Isobe, K. Kimura, M. Kiuchi, S. Okayasu and W. Prusseit, Supercond. Sci. Technol. (2008), 21, 054014

[14] S. Seo, H. Noh, N. Li, J. Jiang, C. Tarantini, R. Shi, S. Jung, M. J. Oh, M. Liu, J. Lee, G. Gu, Y. Jung Jo, T. Park, E. E. Hellstrom, P. Gao and S. Lee, NPG Asia Materials (2020), 12, 7

[15] J. Lu, K. Han, E. S. Choi, Y. Jo, L. Balicas and Y. Xin, J. Appl. Phys. (2007), 101, 123710

[16] S. Arumugam, M. Krishnan, K. Ishigaki, J. Gouchi, R. Pervin, G. Kalai Selvan, P. M. Shirage and Y. Uwatoko, Sci. Rep (2019), 9, 347

[17] J. P.F. Feighan, A. Kursumovic and J. L. MacManus-Driscoll, Supercond. Sci. Technol. (2013), 30, 123001

Footnote:
SuperPower SF4050-AP-i CCT composition: 2 µm silver overlayer; 1.6 µm YBCO layer containing $BaZrO_3$ nano-column artificial pinning centres deposited by metal-organic chemical vapour deposition; 0.2 µm biaxially-textured MgO buffer stack deposited by ion beam assisted deposition; 50 µm Hastelloy substrate
Theva TPL1120 CCT composition: 1 µm silver overlayer; 3.5 µm pure GdBCO layer deposited by pulsed vapour deposition; 3.5 µm biaxially-textured MgO buffer stack deposited by inclined substrate deposition; 50 µm Hastelloy substrate